A Comparison Study of Polypoidal Choroidal Vasculopathy Imaged with Indocyanine Green Angiography and Swept-Source Optical Coherence Tomography Angiography

KIYOUNG KIM, JIN YANG, WILLIAM FEUER, GIOVANNI GREGORI, EUNG SUK KIM, PHILIP J. ROSENFELD, AND SEUNG-YOUNG YU

• PURPOSE: **Indocyanine green angiography (ICGA) was compared with swept-source optical coherence tomography angiography (SS-OCTA) for the detection of polypoidal choroidal vasculopathy (PCV).**

• DESIGN: **Retrospective, cross-sectional.**

• METHODS: **Patients with treatment-naïve PCV based on ICGA imaging underwent same-day SS-OCTA imaging at Kyung Hee University Medical Center between April 2017 and November 2018. ICGA and SS-OCTA images were graded independently. SS-OCTA images were graded using both flow and structural information. Images were graded for the number of polypoidal lesions and the total lesion area, which included both the polypoidal lesions and the branching vascular networks (BVNs).**

• RESULTS: **A total of 31 eyes from 30 patients were enrolled. Polypoidal lesions were identified in all eyes using both modalities, and there was agreement on the number of polypoidal lesions in 17 eyes (55%). In 12 eyes (39%), SS-OCTA graders identified a greater number of polypoidal lesions, and in 2 eyes (6%) ICGA graders identified more lesions. There was no significant difference in the lesion area measurements (standard deviation = 1.09, $P = .08$). The lesion with the largest difference in area measurements resulted from focal areas of atrophy, misdiagnosed as polypoidal lesions on ICGA, and a low-lying serous retinal pigment epithelial detachment erroneously identified as part of the BVN by ICGA graders. SS-OCTA imaging correctly diagnosed the focal areas of atrophy and the serous retinal pigment epitheial detachment.**

• CONCLUSIONS: **SS-OCTA imaging was comparable to ICGA for the diagnosis of treatment-naïve PCV. However, SS-OCTA might be better than ICGA in correctly identifying both polypoidal lesions and BVNs in treatment-naïve PCV. (Am J Ophthalmol 2020;217: 240–251. © 2020 Elsevier Inc. All rights reserved.)**

POLYPOIDAL CHOROIDAL VASCULOPATHY (PCV) IS characterized by a branching vascular network (BVN) that is contiguous with vascular polypoidal lesions.[1,2] It is considered a variant of exudative age-related macular degeneration (AMD). Classic findings on fundus examination include an orange or red subretinal nodule, lipid exudates, and retinal pigment epithelial detachments (PEDs) that may be exudative or hemorrhagic.[3] On indocyanine green angiography (ICGA), both the BVN and the characteristic polypoidal dilatations can be imaged.[4] Because of the pulsatile appearance of some polyps on ICGA and the location of both the BVN and polyps beneath the retinal pigment epithelium (RPE) and above the Bruch membrane, which is the location of typical type 1 macular neovascularization (MNV), an alternative name has been proposed for PCV, which is aneurysmal type 1 MNV.[5]

While ICGA is considered to be the gold standard for the diagnosis of PCV, ICGA is an invasive and time-consuming procedure associated with rare, life-threatening allergic reactions. When ICGA is unavailable and for patients with iodine allergies, the accurate diagnosis of PCV has relied on the combination of fluorescein angiography (FA) and structural imaging with optical coherence tomography (OCT), but the results have varied.[6,7] Chaikitmongkol and associates[8] reported that it is possible to diagnose PCV with 95% sensitivity and specificity using features detected by fundus photography, OCT, and FA without ICGA, so the diagnosis of PCV without using ICGA is possible.[9]

When used alone or in conjunction with other imaging modalities, structural OCT imaging has become a useful tool for the diagnosis of PCV. Multiple, sharply peaked retinal PEDs with an associated double layer sign on OCT B-scans are some helpful features for diagnosing PCV.[10–13] En face OCT has been used as well to diagnose polypoidal lesions.[14] In addition to structural OCT, OCT angiography (OCTA) has reported to be useful

AJO.com Supplemental Material available at AJO.com.
Accepted for publication May 13, 2020.

From the Department of Ophthalmology (K.K., E.S.K., S-Y.Y.), Kyung Hee University Medical Center, Kyung Hee University, Seoul, South Korea, and the Department of Ophthalmology (J.Y., W.F., G.G., P.J.R.), Bascom Palmer Eye Institute, University of Miami Miller School of Medicine, Miami, Florida, USA.

Inquiries to Seung-Young Yu, Department of Ophthalmology, Kyung Hee University Hospital, 23, Kyungheedae-ro, Dongdaemun-gu, Seoul, 02447, South Korea; e-mail: syyu@khu.ac.kr

0002-9394/$36.00
https://doi.org/10.1016/j.ajo.2020.05.017

for the diagnosis of PCV.[15–23] However, most of these studies have used spectral-domain OCTA, which is capable of detecting BVNs in a high percentage of the cases, but the detection of the polypoidal lesions was more variable ranging from 17%-92.3%.[15,18–23]

Compared with spectral-domain OCTA, swept-source OCTA (SS-OCTA) uses a longer wavelength of light that penetrates better through the RPE, has less sensitivity roll-off for imaging sub-RPE structures, and is safer so that a higher laser energy can be used, resulting in images with a better signal-to-noise ratio.[24,25] Moreover, the faster scanning speed allows for denser raster scans for a given field of view and a given amount of chair time compared with spectral-domain OCTA imaging. All these features of SS-OCTA imaging translate into better detection of blood flow for neovascular lesions beneath the RPE.[26–28] Cheung and associates[29] used SS-OCTA to evaluate PCV, and the sensitivities for detection of BVNs and polyps in this report were 77.8% and 40.5%, respectively. Bo and associates[30] showed encouraging results when using SS-OCTA to detect the morphologic characteristics of polypoidal lesions, specifically the tangled vascular structures within the polyps. In these lesions with ICGA-documented polyps, they were able to detect 100% of the BVNs while ICGA detected only 74% of the BVNs. However, in this study, both ICGA and SS-OCTA images were compared side-by-side and the images were superimposed on each other, rather than graded independently, and the results were compared. As a result, further studies are needed to independently compare ICGA and SS-OCTA for the diagnosis of PCV. To determine if SS-OCTA can replace ICGA for the diagnosis of PCV, we independently graded images of treatment-naïve PCV using both modalities and compared the number of polyps and the sizes of the entire polypoidal lesions.

METHODS

PATIENTS WITH TREATMENT-NAÏVE PCV WHO WERE DIAGnosed at the Kyung Hee University Hospital (KHUH) in Seoul, Republic of Korea between April 2017 and November 2018 were included in this retrospective ICGA vs SS-OCTA comparison study. The study was approved by the Institutional Review Board of KHUH. All patients underwent a comprehensive ophthalmologic examination at KHUH and same-day imaging that included FA and ICGA (Spectralis HRA+OCT, Heidelberg Engineering, Heidelberg, Germany) and SS-OCTA (PLEX Elite 9000, Carl Zeiss Meditec, Dublin, California, USA). The SS-OCTA instrument used a central wavelength of 1060 nm and a scan rate of 100,000 A-scans per second. Both 6- × 6-mm and 12- × 12-mm raster images were performed and each scan pattern consisted of 500 A-scans per B-scan at 500 B-scan positions with each B-scan repeated twice at each position for the angiographic imaging, resulting in an A-scan and B-scan separation of 12 μm and 24 μm for the 6- × 6-mm and 12 × 12-mm scans, respectively. The previously described optical microangiography algorithm was used to detect OCT angiographic flow.[31,32]

The diagnosis of PCV was based on the ICGA criteria used in the EVEREST study.[4,33] In this study, massive submacular hemorrhage cases that prevented visualizing active polyps on ICGA were excluded, and in addition cases having other concomitant retinal diseases were excluded. Consensus grading of the ICGA images was performed at KHUH (K.K., S-Y.Y.) without access to FA images or SS-OCTA images. Consensus grading of the SS-OCTA images was performed at the Bascom Palmer Eye Institute (J.Y., P.J.R.) without access to the ICGA images. The number of polypoidal lesions and the combined neovascular lesion area measurements in each eye, which included both the polypoidal and BVN components, were graded on both imaging modalities. All lesions were measured by 2 independent graders without information being available from the other imaging modality. When agreement was not achieved for each imaging modality, a consensus was reached with involvement of a senior adjudicator. On ICGA imaging, polyps were recognized as hyperfluorescent spots on early phase ICGA images that persisted or increased in later phases. The boundary of the BVN was recognized as mottled changes of fluorescence on early phase ICGA that persisted as a plaque or as a discreet vascular network. SS-OCTA grading was based on both en face slabs and B-scans for both the flow and structural images. The en face slabs were produced using boundary layers from the RPE to the RPE-fit. RPE-fit corresponded with the Bruch membrane. These boundary layers were established using the custom segmentation feature on the instrument. The exact position and thickness of the slab were then manually adjusted to optimize the signal for viewing of the PCV complex. The built-in SS-OCTA segmentation editing software was used to manually correct the segmentation boundaries if needed. Both the en face and cross-sectional B-scans, with and without flow, were reviewed to identify all polypoidal lesions and BVNs. Based on overall lesion size, either the 6- × 6-mm or the 12- × 12-mm SS-OCT scan patterns were used to assess the lesion characteristics. Polyps were diagnosed by viewing en face slabs and recognized as foci with flow signals that were associated with dome-shaped, peaked PEDs on the cross-sectional B-scans. BVNs were visualized as vascular networks using both the en face slabs and B-scans with and without superimposition of the flow signal. On B-scans, the diagnosis of a BVN was confirmed by the presence of a double layer sign.[34] Any serous component of a PED was identified using both SS-OCTA en face and B-scan flow and structural images. This serous component was distinguished from a neovascular component of the

TABLE 1. Baseline Demographics and Angiographic Findings of Polypoidal Lesions

Age, years (±SD)	66.8 ± 8.7
Sex (male:female)	2:1
Hypertension (yes:no)	11:19
Polypoidal lesions, n ± SD	
ICGA	2 ± 1
SS-OCTA	2.1 ± 1.2
Area of total PCV lesion, mm^2 ± SD	
ICGA	3.57 ± 3.38
SS-OCTA	3.93 ± 3.19

ICGA = indocyanine green angiography; PCV = polypoidal choroidal vasculopathy; SD = standard deviation; SS-OCTA = swept-source optical coherence tomography angiography.

PED by its hyporeflective content and the absence of a flow signature within the PED.

The total lesion size of the PCV lesion on ICGA imaging was measured manually using the "area tool" embedded in Heidelberg software. The total lesion size of the PCV lesion on SS-OCTA imaging was measured by exporting the en face RPE-RPEfit images in a.tif format and then importing them into Photoshop CS6 (v 13.0.0.0; Adobe, San Jose, California, USA). The lesion was then manually outlined to obtain an area measurement as previously described.[35] ICGA and SS-OCTA were graded using different measuring tools, and therefore the ICGA results were further evaluated using the SS-OCTA grading method for comparison purposes. The graded ICGA images and ungraded structural SS-OCTA images were superimposed using Photoshop CS6. After rotation and rescaling the ICGA images, the registered ICGA images with the grading outlines were reevaluated using SS-OCTA grading method to ensure compatibility of measurements between techniques.

The lesion area measurements obtained from the ICGA and SS-OCTA images were then compared using an analysis of variance (mixed-model analysis of variance). The differences between lesion sizes obtained from these 2 examinations were assessed using Bland-Altman analyses. The total lesion area measurements of the PCV lesion then underwent a square root transformation. This approach eliminated the influence of lesion size on test–retest variability based on lesion size.[36] Statistical analyses were performed with IBM SPSS Statistics for Windows (v 24.0; IBM Corp, Armonk, New York, USA).

RESULTS

FROM APRIL 2017 TO NOVEMBER 2018 IN A SINGLE HOSPITAL, 115 patients were diagnosed as neovascular AMD on ICGA. Of 115 patients with neovascular AMD, 37 patients were classified as PCV based on EVEREST criteria of ICGA. Two patients were excluded because of a history of anti–vascular endothelial growth factor injection, and 5 patients were excluded because they missed SS-OCTA imaging at the same day with ICGA. Therefore, a total of 31 treatment-naïve eyes from 30 patients were included in this study. Baseline demographics and angiographic findings of polypoidal lesions are summarized in Table 1. There was agreement in the number of polypoidal lesions graded in both ICGA and SS-OCTA images in 17 eyes. Examples of this agreement in polypoidal lesions grading between ICGA and SS-OCTA imaging are shown in Figures 1 and 2 and in Supplemental Figures 1 and 2. In these figures, the first row shows the ICGA images before and after grading of the polypoidal lesions and the total lesion area when viewed from the left to the right columns, respectively. The second row shows SS-OCTA en face flow images of the RPE-RPEfit slab before grading and after grading of the polypoidal lesions and the total lesion area when viewed from the left to the right columns, respectively. The third row shows the en face structural image of SS-OCTA RPE-RPEfit slab, representative B-scans showing the structure of polypoidal lesions and BVN with superimposed segmentation lines and color-coded flow, followed by an image of the entire neovascular lesion (polyps plus BVN) filled in blue with any serous component of the PED highlighted in yellow.

There was disagreement in the number of polypoidal lesions graded in both ICGA and SS-OCTA images in 14 eyes. Twelve eyes had a greater number of polypoidal lesions graded on SS-OCTA than ICGA images. Figure 3 and Supplemental Figure 3 show examples of polypoidal lesions identified on SS-OCTA that were missed on ICGA. Two eyes were graded as having more polypoidal lesions by ICGA than SS-OCTA imaging (Figure 4, Supplemental Figure 4). Figure 4, B shows 1 case in which 4 polypoidal lesions were identified on the ICGA while only 1 polypoidal lesion was identified on SS-OCTA. The 3 polypoidal lesions missed by the SS-OCTA graders were actually areas of hypertransmission on OCT imaging consistent with focal areas of evolving RPE atrophy as shown by the SS-OCTA en face sub-RPE slab images and corresponding B-scans (Figure 4, J-M). This case shows that these areas with evolving RPE atrophy can masquerade as polyps on ICGA imaging. Thus, the SS-OCTA graders did not miss polypoidal lesions but correctly graded for the absence of polypoidal lesions. This case also shows a dramatic difference between ICGA and SS-OCTA graders in the assessment that of total lesion area (Figure 4, C, F, and I). By comparing the grading results from the ICGA and SS-OCTA images, the area of the BVN outlined on the ICGA images corresponds with a shallow RPE elevation on the SS-OCTA images that appears to be a serous PED. Thus, a serous PED on ICGA imaging can masquerade as a BVN (Figure 4, E and H). This case corresponds with the outlier labeled with the black arrow in Figure 5, which had the largest difference in the square

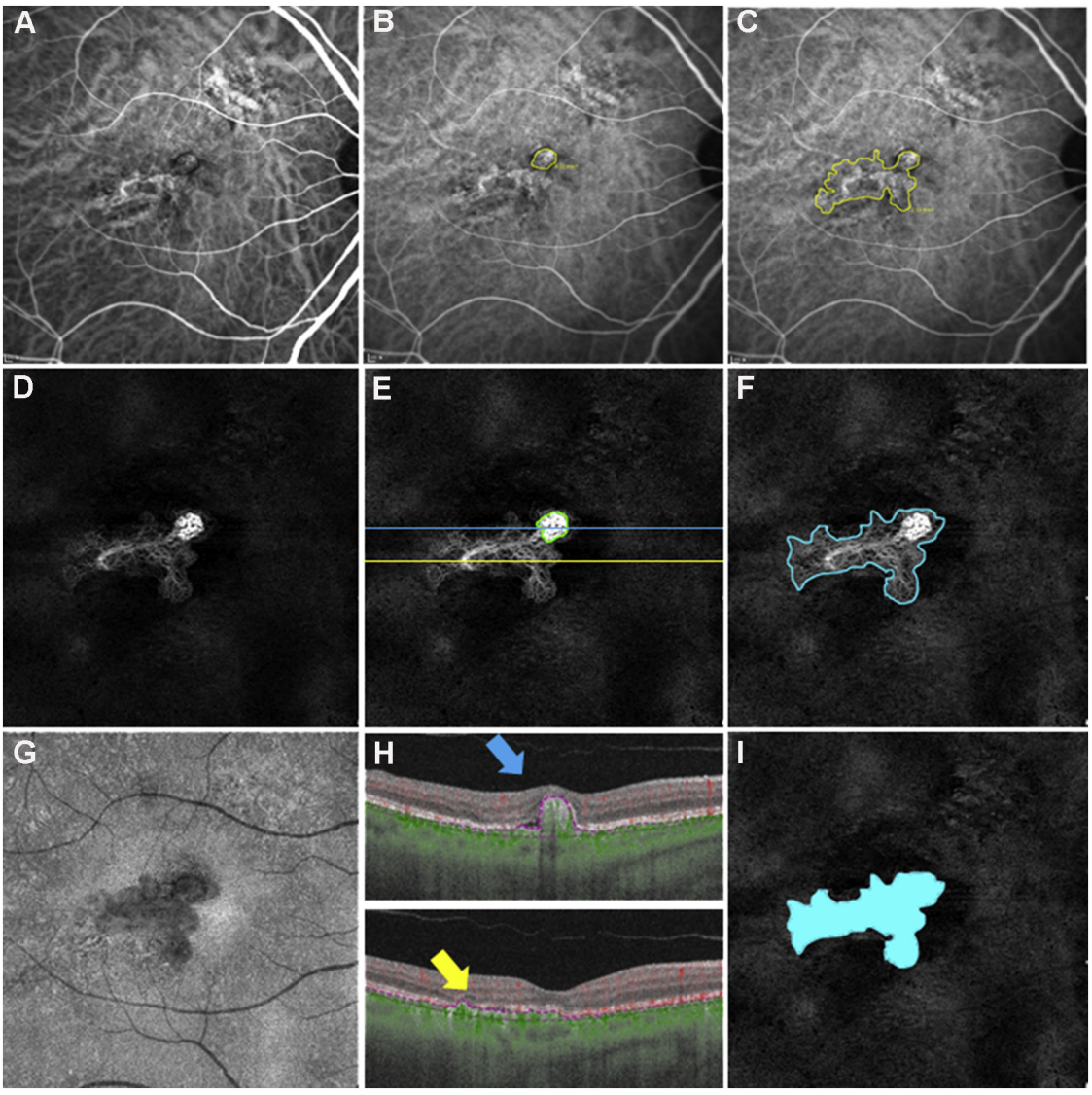

FIGURE 1. Polypoidal choroidal vasculopathy (PCV) lesion with consistent findings and similar area measurements on both indocyanine green angiography (ICGA) and swept-source optical coherence tomography angiography (SS-OCTA) imaging. A. ICGA image before grading. B. One polyp was detected and outlined on the ICGA image. C. Outline of polyp with branching vascular network (BVN) on the ICGA image. D. SS-OCTA 6- × 6-mm en face flow image using a slab from the retinal pigment epithelium (RPE) to the Bruch membrane showing the entire PCV lesion before grading. E. One polyp was detected and outlined on the SS-OCTA image. Tangle vessel structures within this polyp can be visualized by SS-OCTA imaging. F. Outline of polyp and BVN on the SS-OCTA image. G. The SS-OCTA en face structure image that uses the same boundary segmentations as for the slab flow images depicted in panels D through F reveals a hyporeflective contour that corresponds with the entire PCV lesion. H. B-scans corresponding with the lines shown in panel E with superimposed RPE to Bruch membrane segmentation boundaries and color-coded flow showing the structures of the polyp (blue arrow) and BVN (yellow arrow). I. Color-coded grading of the entire PCV lesion, which included polyps plus BVN colored in blue.

root area measurements. The second case in which there was disagreement in the number of polypoidal lesions between ICGA and SS-OCTA imaging is shown in Supplemental Figure 4. While 3 polypoidal lesions were identified by ICGA graders (Supplemental Figure 4, B), only 1 polypoidal lesion was identified by SS-OCTA graders (Supplemental Figure 4, E). However, a lacy, fan-shaped lesion located between 3 polypoidal lesions on the ICGA image was regarded as type 1 MNV by ICGA graders. ICGA graders did not identify the largest polyp, which was identified by the SS-OCTA graders on the temporal side of fovea based on the configuration of the PED and the internal tangled vessel appearance of the PED.

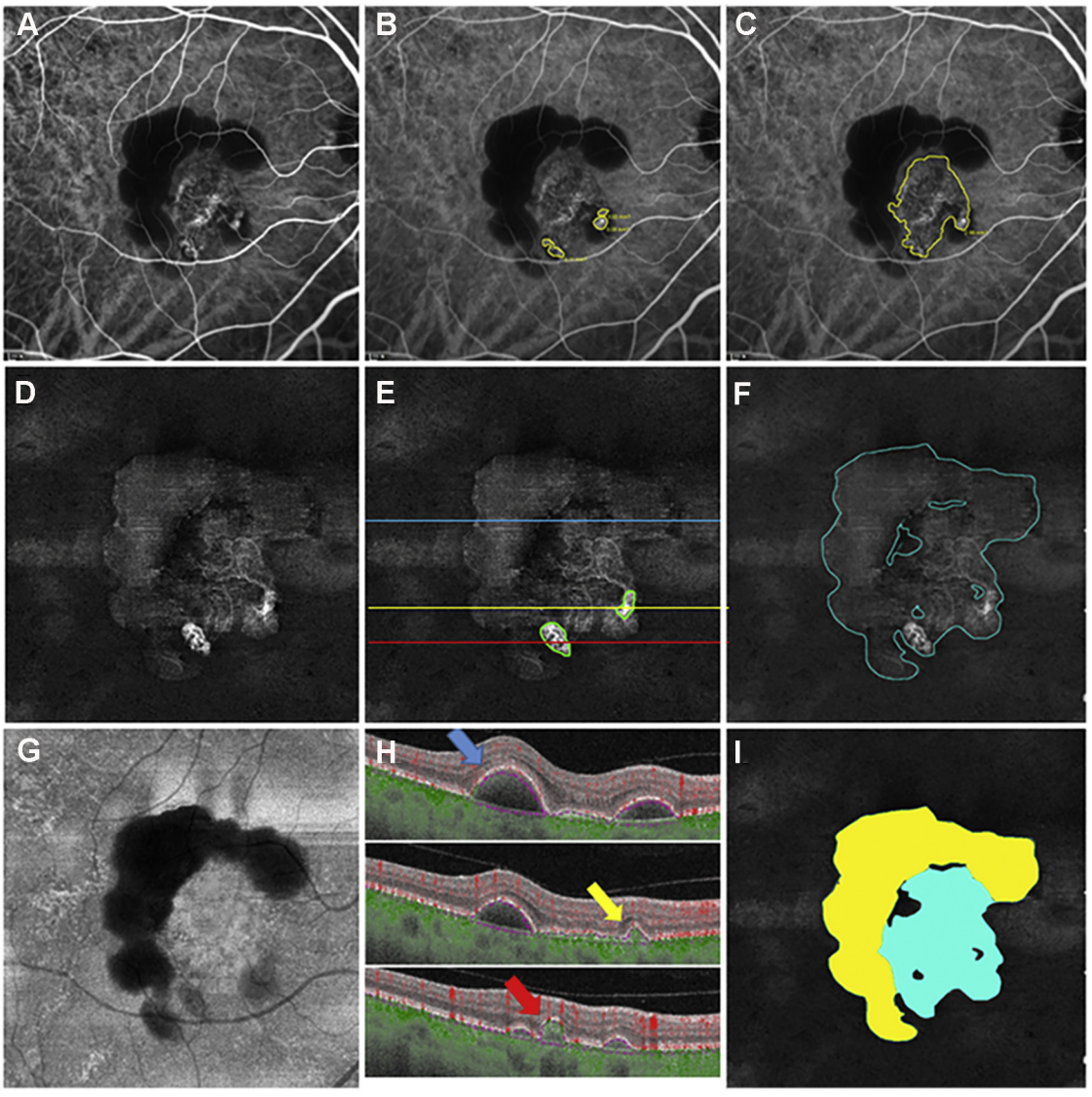

FIGURE 2. Polypoidal choroidal vasculopathy (PCV) lesion with consistent findings and similar area measurements on both indocyanine green angiography (ICGA) and swept-source optical coherence tomography angiography (SS-OCTA) imaging. A. ICGA image before grading. B. Two polyps were detected and outlined on the ICGA image. C. Outline of polyps with branching vascular network (BVN) on the ICGA image. D. SS-OCTA 6- × 6-mm en face flow image using a slab from the retinal pigment epithelium (RPE) to the Bruch membrane showing the entire PCV lesion before grading. E. Two polyps were detected and outlined on the SS-OCTA image. Tangle vessels within 1 of the polyps can be visualized by SS-OCTA imaging. F. Outline of polyp and BVN on the SS-OCTA image. G. The SS-OCTA en face structure image that uses the same boundary segmentation as for the slab flow images depicted in panels D through F reveals a hyporeflective contour that corresponds with the entire PCV lesion with the darkest area corresponding with the serous component of the RPE detachment. H. B-scans corresponding with the lines shown in panel E with superimposed segmentation boundaries from the RPE to Bruch membrane and color-coded flow showing the structures of the serous PED (blue arrow), polyps (yellow and red arrows), and the BVN. I. Color-coded grading of the entire PCV lesion, which included polyps plus BVN colored in blue with the serous component of the PED highlighted in yellow.

The difference in the mean PCV lesion area measurements between ICGA and SS-OCTA was 0.35 mm^2, and this difference was not statistically significant (standard deviation [SD] = 1.09, $P = .08$; Figure 5, A). However, when the square root transformation strategy was used, the difference between the area measurements was 0.12 mm and this difference, while statistically significant (SD = 0.31, $P = .042$), was not clinically significant (Figure 5, B). Figure 5 shows that this significance was driven by a single case (black arrow) that showed greater separation from the other measurements after the square root transformation and the ICGA area measurement of this case was

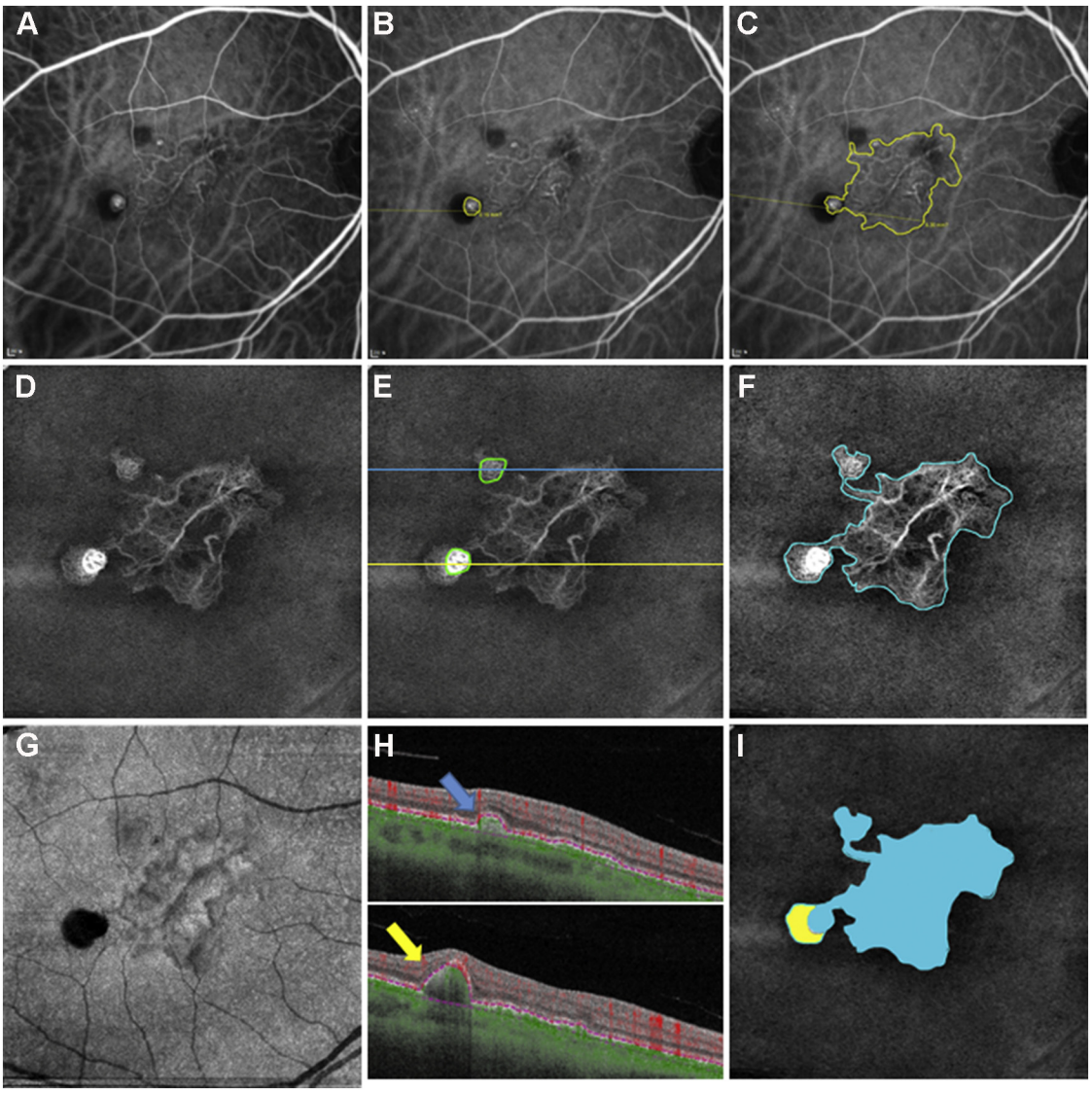

FIGURE 3. Polypoidal choroidal vasculopathy (PCV) lesion with more polyps identified on swept-source optical coherence tomography angiography (SS-OCTA) compared with indocyanine green angiography (ICGA). A. ICGA image before grading. B. A single polyp was detected and outlined on the ICGA image, although the image does reveal a small fluorescent dot that was not graded as a polyp. C. Outline of polyp with branching vascular network (BVN) on the ICGA image. D. SS-OCTA 6- × 6-mm en face flow image using a slab from the retinal pigment epithelium (RPE) to the Bruch membrane showing the entire PCV lesion before grading. E. Two polyps were detected and outlined on the SS-OCTA image. Tangle vessels within both polyps are visualized by SS-OCTA imaging. F. Outline of polyps and BVN on the SS-OCTA image. G. The SS-OCTA en face structure image that uses the same boundary segmentation as for the slab flow images depicted in panels D through F reveals a hyporeflective contour that corresponds with the entire PCV lesion with the darkest area corresponding with the serous component of the RPE detachment. H. B-scans corresponding with the lines shown in panel E with superimposed segmentation boundaries from the RPE to Bruch membrane and color-coded flow showing the 2 polyps (blue and yellow arrows) and BVN. I. Color-coded grading of the entire PCV lesion, which included polyps plus BVN colored in blue with the small serous component of the PED highlighted in yellow.

subsequently shown to be incorrect (Figure 4). Bland-Altman analyses demonstrated the magnitude of the differences in these area measurements with or without subretinal fluid (SRF). The red data points in Figure 5 represent the 19 eyes that had variable amounts of SRF, and 6 of these 19 eyes had subretinal hemorrhage. The eyes with the largest differences in area measurements appear to be the ones with SRF, but these differences between eyes with and without SRF was not statistically significant (Figure 5, C; $P = .29$). This difference was still not statistically significant with the square root transformation (Figure 5, D; $P = .13$). The absolute value of the area

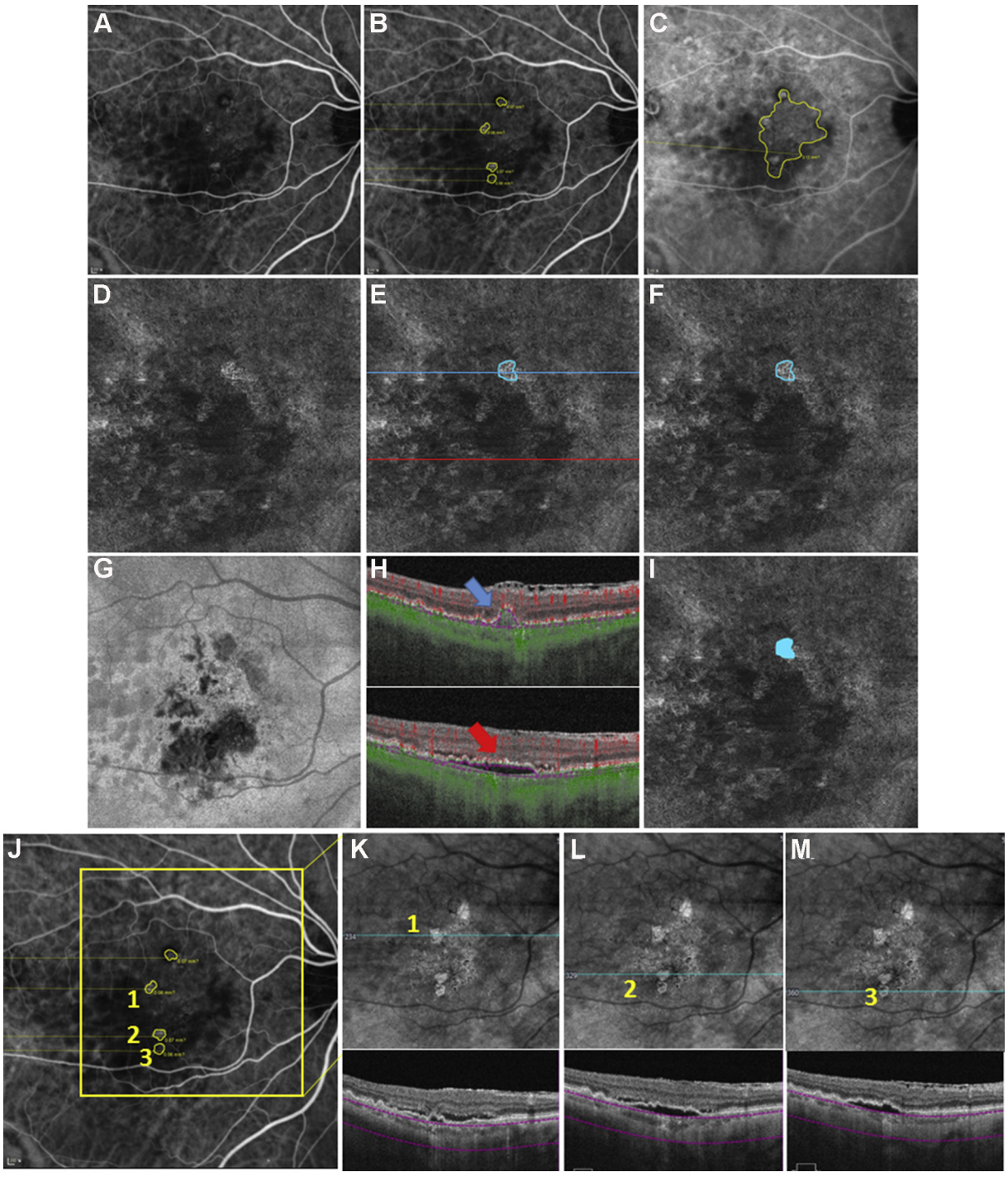

FIGURE 4. Polypoidal choroidal vasculopathy (PCV) lesion showing disagreement in grading between swept-source optical coherence tomography angiography (SS-OCTA) and indocyanine green angiography (ICGA) due to the erroneous diagnosis of polyps on ICGA imaging. A. ICGA image before grading. B. Four polyps were detected and outlined on the ICGA image. C. Outline of the polyps with the associated branching vascular network (BVN) on the ICGA image. D. SS-OCTA 6- × 6-mm en face flow image using a slab from the retinal pigment epithelium (RPE) to the Bruch membrane showing the entire PCV lesion before grading. E. A single polyp was detected and outlined on the SS-OCTA image. F. Outline of the polyp, but a BVN was not detected on the SS-OCTA image. G. The SS-OCTA en face structure image that uses the same boundary segmentation as for the slab flow images depicted in panels D through F reveals multiple hyporeflective contours that correspond with the polyp and to area of a low-lying serous RPE detachment. H. B-scans corresponding with the lines shown in panel E with superimposed segmentation boundaries from the RPE to Bruch

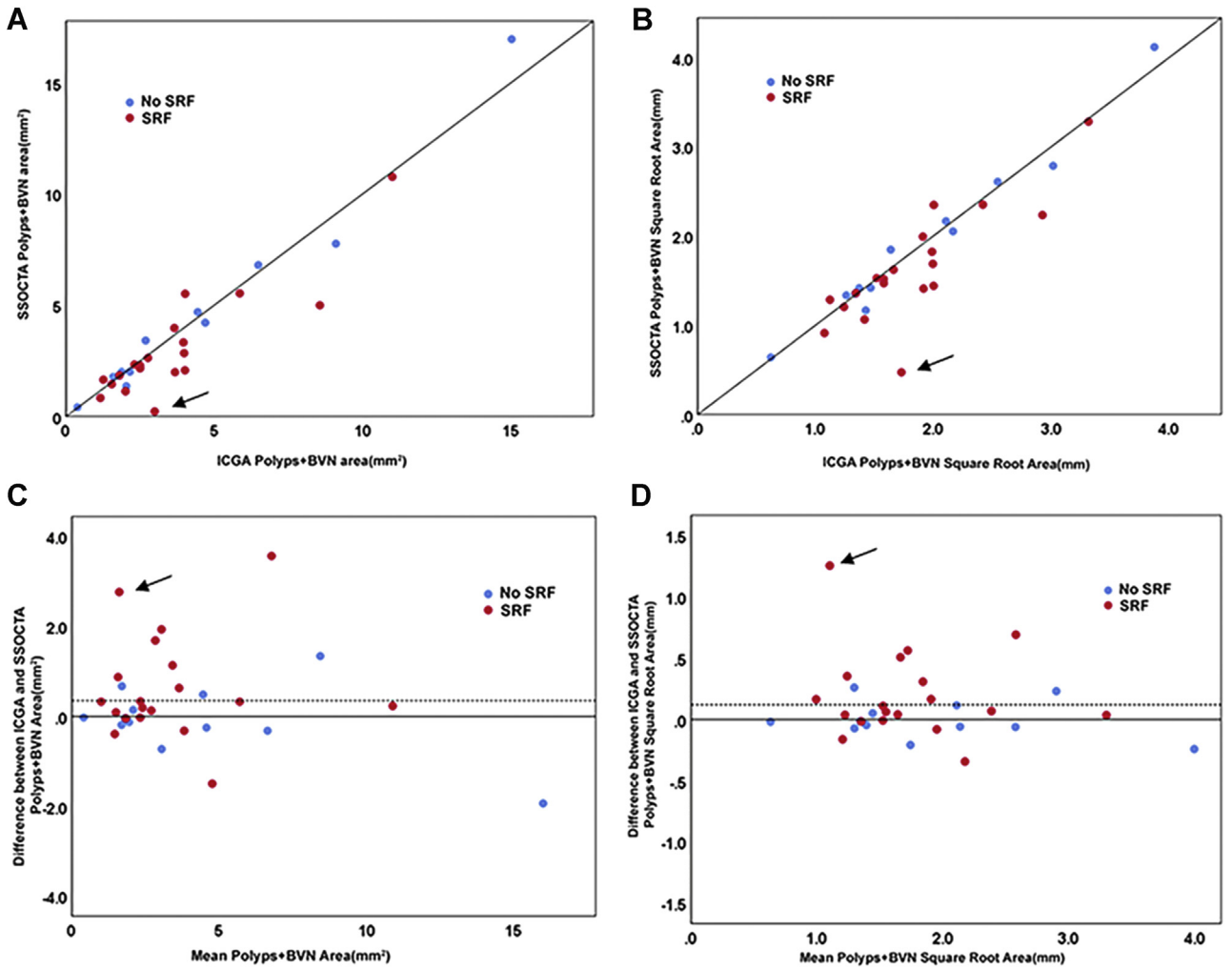

FIGURE 5. Comparison between the area and the square-root area measurements of polyps and branching vascular networks (BVNs) using swept-source optical coherence tomography angiography (SS-OCTA) and indocyanine green angiography (ICGA) imaging. A. Scatterplots comparing area measurements. On average, the ICGA polyps and BVN area measurements are 0.35 mm^2 larger than SS-OCTA measurements (standard deviation [SD] = 1.09; P = .08). B. Scatterplots comparing the square root area measurements. On average, the ICGA polyps and BVN area measurements are 0.12 mm larger than SS-OCTA measurements (SD = 0.31; P = .042). C. Bland-Altman analysis showing the difference in area measurements of polyps and BVNs from SS-OCTA and ICGA with or without subretinal fluid (SRF). The differences look larger for lesions with SRF, but the differences were not significant (P = .29, t test). D. Bland-Altman analysis showing the differences in square root area measurements of polyps and BVNs from SS-OCTA and ICGA with or without SRF (P = .13, t test). The case labeled with a black arrow shows a larger difference compared with the other eyes after the square root area transformation.

difference measurements became less after the square root transformation for all cases except the one highlighted by the black arrow in Figure 5, D, which was the same eye designated by the arrow in Figure 5, B.

On SS-OCTA imaging, SRF was identified in 19 of 31 eyes, and 6 of these 19 eyes had subretinal hemorrhages. Supplemental Figure 5 shows a case with dense subretinal hemorrhages. Even in the presence of subretinal hemorrhages, SS-OCTA en face and B-scan images can detect the polypoidal lesions, the BVNs, and serous PEDs. Moreover SS-OCTA imaging can detect the presence of type 2 neovascularization arising from the BVN, which is a variant of type 1 neovascularization. Two of the 31 eyes were found to have combined type 1 and type 2 neovascular lesions as detected by SS-OCTA, which is difficult to detect using ICGA alone (Supplemental Figure 6).

membrane and color-coded flow showing 1 polyp (blue arrow) and a low-lying serous RPE detachment. I. Color-coded grading of the entire PCV lesion, which only includes a polyp colored in blue. J. The 3 polyps designated as 1, 2, and 3 on ICGA image correspoding to the regions of focal choroidal hypertransmission on SS-OCTA images. K through M. En face structural images from SS-OCTA sub-RPE slabs and corresponding B-scans depicting the absence of polyps and the presence of choroidal hypertransmission.

DISCUSSION

WHILE ICGA IS CURRENTLY THE GOLD STANDARD FOR THE diagnosis of PCV, this report shows that SS-OCTA appears to be at least as good and possibly better at accurately diagnosing all the components of a PCV lesion when both flow and structural information from the SS-OCTA scans are used to identify the total PCV lesion. Moreover, SS-OCTA imaging is safer, faster, less time-consuming, less expensive for the patient, and more easily repeated at follow-up visits compared with ICGA. While SS-OCTA is routinely thought of as a replacement for FA imaging,[37,38] this current study, along with our previous report showing the benefits of SS-OCTA for the detection of subclinical, nonexudative type 1 MNV, suggests that SS-OCTA may be able to replace ICGA for the clinical care of treatment-naïve patients with neovascular PCV.

We showed comparable outcomes not only with respect to total lesion size but also for the number of polypoidal lesions detected using both imaging modalities. Our results differ from previous reports in which the detection rates of polyps using OCTA have been variable.[18–23] A possible explanation for the differences in polyp detection between ICGA and OCTA may be the different ICG angiographic criteria used to diagnose PCV in the different studies. However, it is more likely that the variability was due to the OCTA strategies used to detect PCV. Detection of PCV using OCTA is multifactorial and depends on the instruments (spectral-domain OCTA vs SS-OCTA), the different segmentation strategies, and the different OCT angiographic flow detection algorithms. The sensitivities for detection of polyps in a study by Cheung and associates[29] was only 40.5% using a different SS-OCTA instrument,[29] while Bo and associates[30] reported 100% polypoidal lesions detection when using the same SS-OCTA instrument that was used in our current study. In addition to using a different SS-OCTA instrument, the major difference in the former study is that grading for SS-OCTA was performed using only en face flow information while we incorporated both flow and structural information. Moreover, we reviewed all the structural B-scans to ensure that the segmentation lines followed the appropriate boundaries for the identification of the RPE and the Bruch membrane. Failure of the RPE segmentation algorithm in eyes with polypoidal lesions that have multiple, irregularly shaped PEDs can occur, especially in the presence of hemorrhages. Manual adjustment of the RPE segmentation boundary may be needed, as performed in our study for the accurate detection of polypoidal lesions. More recently, Fujita and associates[39] reported accuracy of 92.6% for counting polypoidal lesions with SS-OCTA relative to ICGA. The major difference is that they initially used flow signal in SS-OCTA B-scans to detect polyps, and only graded OCTA findings independently and then performed head-to-head comparisons with ICGA. Both structural OCT B-scans and en face OCT images were used for the detection of polypoidal lesions once the segmentation lines were edited. Moreover, the use of en face imaging of the structural OCT scans can often identify the full extent of the BVN demarcated by the hyporeflective polypoidal structures at the margins as shown in the figures. For example, the detection rate of polyps by OCTA ranged from 75.2% reported by Takayama and associates[23] to 92.3% reported by Wang and associates[22] in which they performed manual segmentation. In Chu-Hsuan and associates,[40] manual adjustment of the segmentation lines increased the identification rate of polyps from 62% to 86%. This grading approach is consistent with clinical practice in which OCTA images are interpreted together with structural OCT information and segmentation lines should always be checked for accuracy.

In the current study, the total lesion size measurements of the PCV lesions were compared after independently grading the ICGA and SS-OCTA images. The total lesion size in this study included the size of the polypoidal lesions plus the BVN. Based on the characteristics of PCV lesions, most of the total PCV lesion size was determined by the size of the BVN. In previous reports using OCTA imaging in eyes with ICGA-confirmed PCV, BVNs were detected in 70%-100% of cases.[5,15,18,20,22,30] In our study, we detected BVNs in all cases and there was no significant difference in PCV lesion area measurements between the ICGA images and SS-OCTA images. While the difference became significant using the square root transformation strategy, this significance was driven by a single case (Figure 5, black arrow) in which the SS-OCTA images more accurately defined the PCV lesion compared with the ICGA images due to the presence of a serous PED that was erroneously graded as a BVN (Figure 4).

To optimize the visualization of the PCV complex in our study, we manually adjusted the thickness and location of the slab. Some automated segmentation lines were manually adjusted when the line failed to accurately follow the RPE. As a result, SS-OCTA was able to detect all the polypoidal lesions detected by ICGA except in 2 cases (Figure 4, Supplemental Figure 4). These 2 cases had fewer polypoidal lesions detected by SS-OCTA imaging, but in both cases, SS-OCTA imaging provided additional structural details that helped identify real polyps and distinguish real polyps from areas masquerading as polyps on ICGA imaging. In 1 case (Figure 4), 3 polyps identified by ICGA corresponded with regions of incomplete RPE atrophy characterized by hypertransmission into the choroid as seen on OCT B-scans.[41] RPE window defects, which are caused by RPE atrophy, were initially misdiagnosed as polyps and have been reported in the EVEREST study.[4] In the second case (Supplemental Figure 4), SS-OCTA missed 3 small polypoidal lesions adjacent to a much larger polypoidal lesion on the temporal side of the fovea that was considered to be part of the BVN by the ICGA graders. In

12 cases in this study, SS-OCTA was able to reveal more of the polypoidal structure than is typically revealed with ICGA imaging. The main reason for the difference was that majority of polyps hidden from PEDs or subretinal hemorrhages can be better visualized by SS-OCTA. In 3 of 12 cases, SS-OCTA graders detected more polypoidal lesions on the lesions regarded as aneurysmal budding from the BVN, and these lesions did not satisfy the EVEREST ICGA criteria for polyps. This outcome shows the need to revise the EVEREST criteria based on information from SS-OCTA and the need to develop consensus criteria for the grading of PCV using SS-OCTA imaging.

With recent advances in OCTA instrumentation, the structural details of polypoidal lesions have received increased attention by retinal specialists. Some consider these polypoidal lesions to be aneurysmal dilatations of neovascular tissue, similar to aneurysms in the systemic circulation.[5] However, aneurysmal structures were not common in our case series. Other terminology, such as rosettes, networks, and clusters, have also been used to describe the OCTA appearances of polyps.[17] Recently, the term "tangled vascular structures" has been used to describe polypoidal lesions by Bo and associates,[30] and our results are more consistent with their observations. Most of the polypoidal lesions in this study consisted of tangled vessels with a variety of configurations. The tangled vascular structures can be observed better in the SS-OCTA images of larger polypoidal lesion as shown in Supplemental Figure 2, while the ICGA images are more ambiguous. Yuzawa and associates[42] showed that the tangled vessels could be visible as a ring of hyperfluorescence on ICGA when the dye fades. In addition, SS-OCTA imaging was able to identify the type 2 neovascular component of PCV lesions that could be missed using ICGA alone. Using different boundary-specific segmentation strategies, we have been able to distinguish type 1 MNV from type 2 MNV in eyes with exudative AMD.[43] The type 1 component was identified by using a slab extending from the RPE to the RPEfit (Bruch membrane) boundary, and the type 2 component of the MNV was visualized using a slab extending from the outer plexiform layer to the RPE. We used the same segmentation strategy in this PCV grading comparison study and detected 2 cases that had type 1 and type 2 MNV in the same PCV complex, while ICGA was not be able to distinguish these lesion characteristics.

As previously mentioned, SS-OCTA has several advantages over conventional angiography. These include rapid acquisition time, frequent noninvasive repeated scans, and the ability to visualize blood flow at high resolution within different segmentation slabs. Deeper scans can also provide more information about the choriocapillaris and choroidal layers.[44,45] The limitations of SS-OCTA imaging include reduced image quality due to motion artifacts, which usually result when patients have poor visual acuity and are unable to focus on the target during image acquisition and the presence of a highly elevated PED in which accurate segmentation the boundary detection algorithms fail. However, this limitation can be improved with the use of manual segmentation correction.

The limitation of this study is its relatively small sample size and that all the PCV cases were diagnosed based on ICGA findings before the SS-OCTA images were reviewed so SS-OCTA graders knew that polypoidal lesions and BVNs were present in each case. As a result, the sensitivity and specificity of PCV detection by SS-OCTA was not applied. In addition, the performance of flow information alone from the SS-OCTA images cannot be compared with ICGA because this study considered both flow and structural information from the SS-OCTA scans when grading PCV. However, larger studies using SS-OCTA in the diagnosis of PCV in the future will be useful in ultimately determining the diagnostic value of this technology.

CONCLUSIONS

OUR FINDINGS SUGGEST THAT BY USING BOTH FLOW AND structural information from SS-OCTA scans SS-OCTA imaging should be able to replace ICGA imaging for the routine diagnosis and follow-up of eyes with PCV. The BVN and polypoidal components were well visualized in all eyes. Even in eyes with large PEDs or dense subretinal hemorrhages, the PCV complex could still be identified using SS-OCTA. Moreover, SS-OCTA can also provide additional structural details that help distinguish real polyps from lesions masquerading as polyps. Overall, the measurements of the PCV lesions were comparable between ICGA and SS-OCTA examinations. Using both flow and structural SS-OCT imaging, we were able to highlight morphologic characteristics of PCV lesions that could not be fully appreciated using routine ICGA images.

ALL AUTHORS HAVE COMPLETED AND SUBMITTED THE ICMJE FORM FOR DISCLOSURE OF POTENTIAL CONFLICTS OF INTEREST. Funding/Support: The authors indicate no financial support. Financial Disclosures: G.G. and P.J.R. received research support from Carl Zeiss Meditec, Inc. G.G. and the University of Miami co-own a patent that is licensed to Carl Zeiss Meditec, Inc. P.J.R. also received additional research support from Stealth Biotherapeutics and Boehringer-Ingelheim. He is a consultant for Apellis, Boehringer-Ingelheim, Carl Zeiss Meditec, Chengdu Kanghong Biotech, Ocunexus Therapeutics, Ocunexus, Ocudyne, and Unity Biotechnology. P.J.R. has equity interest in Apellis, Verana Health, and Ocudyne. S-Y.Y. received research support from Allergan, Bayer, Norvatis, Carl Zeiss Meditec, and Heiderberg Enginerging. J.Y., W.F., K.K., and E.S.K. indicate no financial conflicts of interest. All authors attest that they meet the current ICMJE criteria for authorship.

REFERENCES

1. Imamura Y, Engelbert M, Iida T, Freund KB, Yannuzzi LA. Polypoidal choroidal vasculopathy: a review. *Surv Ophthalmol* 2010;55(6):501–515.
2. Cheung CMG, Lai TYY, Ruamviboonsuk P, et al. Polypoidal choroidal vasculopathy: definition, pathogenesis, diagnosis, and management. *Ophthalmology* 2018;125(5):708–724.
3. Koh AH, Expert PCVP, Chen LJ, et al. Polypoidal choroidal vasculopathy: evidence-based guidelines for clinical diagnosis and treatment. *Retina* 2013;33(4):686–716.
4. Tan CS, Ngo WK, Lim LW, Tan NW, Lim TH, Group ES. EVEREST study report 3: diagnostic challenges of polypoidal choroidal vasculopathy. Lessons learnt from screening failures in the EVEREST study. *Graefes Arch Clin Exp Ophthalmol* 2016;254(10):1923–1930.
5. Inoue M, Balaratnasingam C, Freund KB. Optical coherence tomography angiography of polypoidal choroidal vasculopathy and polypoidal choroidal neovascularization. *Retina* 2015;35(11):2265–2274.
6. Spaide RF, Klancnik JM Jr, Cooney MJ. Retinal vascular layers imaged by fluorescein angiography and optical coherence tomography angiography. *JAMA Ophthalmol* 2015;133(1):45–50.
7. Tan CS, Ngo WK, Lim LW, Tan NW, Lim TH. EVEREST study report 4: fluorescein angiography features predictive of polypoidal choroidal vasculopathy. *Clin Exp Ophthalmol* 2019;47(5):614–620.
8. Chaikitmongkol V, Kong J, Khunsongkiet P, et al. Sensitivity and specificity of potential diagnostic features detected using fundus photography, optical coherence tomography, and fluorescein angiography for polypoidal choroidal vasculopathy. *JAMA Ophthalmol* 2019;137(6):661–667.
9. Cheung CMG, Kim JE. Diagnosing polypoidal choroidal vasculopathy without indocyanine green angiography. *JAMA Ophthalmol* 2019;137(6):667–668.
10. Sengupta S, Surti R, Vasavada D. Sensitivity and specificity of spectral-domain optical coherence tomography in detecting idiopathic polypoidal choroidal vasculopathy. *Am J Ophthalmol* 2015;160(1):203–204.
11. De Salvo G, Vaz-Pereira S, Keane PA, Tufail A, Liew G. Sensitivity and specificity of spectral-domain optical coherence tomography in detecting idiopathic polypoidal choroidal vasculopathy. *Am J Ophthalmol* 2014;158(6):1228–1238.
12. Liu R, Li J, Li Z, et al. Distinguishing polypoidal choroidal vasculopathy from typical neovascular age-related macular degeneration based on spectral domain optical coherence tomography. *Retina* 2016;36(4):778–786.
13. Chang YS, Kim JH, Kim JW, Lee TG, Kim CG. Optical coherence tomography-based diagnosis of polypoidal choroidal vasculopathy in Korean patients. *Korean J Ophthalmol* 2016;30(3):198–205.
14. Kokame GT, Shantha JG, Hirai K, Ayabe J. En face spectral-domain optical coherence tomography for the diagnosis and evaluation of polypoidal choroidal vasculopathy. *Ophthalmic Surg Lasers Imaging Retina* 2016;47(8):737–744.
15. Tanaka K, Mori R, Kawamura A, Nakashizuka H, Wakatsuki Y, Yuzawa M. Comparison of OCT angiography and indocyanine green angiographic findings with subtypes of polypoidal choroidal vasculopathy. *Br J Ophthalmol* 2017;101(1):51–55.
16. de Carlo TE, Kokame GT, Shantha JG, Lai JC, Wee R. Spectral-domain optical coherence tomography angiography for the diagnosis and evaluation of polypoidal choroidal vasculopathy. *Ophthalmologica* 2018;239(2-3):103–109.
17. Seong S, Choo HG, Kim YJ, et al. Novel findings of polypoidal choroidal vasculopathy via optical coherence tomography angiography. *Korean J Ophthalmol* 2019;33(1):54–62.
18. Teo KYC, Cheung GCM. New concepts in polypoidal choroidal vasculopathy imaging: a focus on optical coherence tomography and optical coherence tomography angiography. *Asia Pac J Ophthalmol (Phila)* 2019; https://doi.org/10.22608/APO.201909. [Epub ahead of print].
19. Kim JY, Kwon OW, Oh HS, Kim SH, You YS. Optical coherence tomography angiography in patients with polypoidal choroidal vasculopathy. *Graefes Arch Clin Exp Ophthalmol* 2016;254(8):1505–1510.
20. Srour M, Querques G, Semoun O, et al. Optical coherence tomography angiography characteristics of polypoidal choroidal vasculopathy. *Br J Ophthalmol* 2016;100(11):1489–1493.
21. Tomiyasu T, Nozaki M, Yoshida M, Ogura Y. Characteristics of polypoidal choroidal vasculopathy evaluated by optical coherence tomography angiography. *Invest Ophthalmol Vis Sci* 2016;57(9):324–330.
22. Wang M, Zhou Y, Gao SS, et al. Evaluating polypoidal choroidal vasculopathy with optical coherence tomography angiography. *Invest Ophthalmol Vis Sci* 2016;57(9):526–532.
23. Takayama K, Ito Y, Kaneko H, et al. Comparison of indocyanine green angiography and optical coherence tomographic angiography in polypoidal choroidal vasculopathy. *Eye (Lond)* 2017;31(1):45–52.
24. Miller AR, Roisman L, Zhang Q, et al. Comparison between spectral-domain and swept-source optical coherence tomography angiographic imaging of choroidal neovascularization. *Invest Ophthalmol Vis Sci* 2017;58(3):1499–1505.
25. Rebhun CB, Moult EM, Novais EA, et al. Polypoidal choroidal vasculopathy on swept-source optical coherence tomography angiography with variable interscan time analysis. *Transl Vis Sci Technol* 2017;6(6):4.
26. Ting DS, Cheung GC, Lim LS, Yeo IY. Comparison of swept source optical coherence tomography and spectral domain optical coherence tomography in polypoidal choroidal vasculopathy. *Clin Exp Ophthalmol* 2015;43(9):815–819.
27. Dansingani KK, Balaratnasingam C, Naysan J, Freund KB. En face imaging of pachychoroid spectrum disorders with swept-source optical coherence tomography. *Retina* 2016;36(3):499–516.
28. Bakthavatsalam M, Ng DS, Lai FH, et al. Choroidal structures in polypoidal choroidal vasculopathy, neovascular age-related maculopathy, and healthy eyes determined by binarization of swept source optical coherence tomographic images. *Graefes Arch Clin Exp Ophthalmol* 2017;255(5):935–943.
29. Cheung CMG, Yanagi Y, Mohla A, et al. Characterization and differentiation of polypoidal choroidal vasculopathy using swept source optical coherence tomography angiography. *Retina* 2017;37(8):1464–1474.
30. Bo Q, Yan Q, Shen M, et al. Appearance of polypoidal lesions in patients with polypoidal choroidal vasculopathy using swept-source optical coherence tomographic angiography. *JAMA Ophthalmol* 2019;137(6):642–650.

31. Huang Y, Zhang Q, Thorell MR, et al. Swept-source OCT angiography of the retinal vasculature using intensity differentiation-based optical microangiography algorithms. *Ophthalmic Surg Lasers Imaging Retina* 2014;45(5):382–389.
32. Wang RK, An L, Francis P, Wilson DJ. Depth-resolved imaging of capillary networks in retina and choroid using ultrahigh sensitive optical microangiography. *Opt Lett* 2010;35(9):1467–1469.
33. Koh A, Lee WK, Chen LJ, et al. EVEREST study: efficacy and safety of verteporfin photodynamic therapy in combination with ranibizumab or alone versus ranibizumab monotherapy in patients with symptomatic macular polypoidal choroidal vasculopathy. *Retina* 2012;32(8):1453–1464.
34. Shi Y, Motulsky EH, Goldhardt R, et al. Predictive value of the OCT double-layer sign for identifying subclinical neovascularization in age-related macular degeneration. *Ophthalmol Retina* 2019;3(3):211–219.
35. Yehoshua Z, Rosenfeld PJ, Gregori G, et al. Progression of geographic atrophy in age-related macular degeneration imaged with spectral domain optical coherence tomography. *Ophthalmology* 2011;118(4):679–686.
36. Uyama M, Wada M, Nagai Y, et al. Polypoidal choroidal vasculopathy: natural history. *Am J Ophthalmol* 2002;133(5):639–648.
37. Roisman L, Zhang Q, Wang RK, et al. Optical coherence tomography angiography of asymptomatic neovascularization in intermediate age-related macular degeneration. *Ophthalmology* 2016;123(6):1309–1319.
38. de Oliveira Dias JR, Zhang Q, Garcia JMB, et al. Natural history of subclinical neovascularization in nonexudative age-related macular degeneration using swept-source OCT angiography. *Ophthalmology* 2018;125(2):255–266.
39. Fujita A, Kataoka K, Takeuchi J, et al. Diagnostic characteristics of polypoidal choroidal vasculopathy based on B-scan swept-source optical coherence tomography angiography and its interrater agreement compared with indocyanine green angiography. *Retina* 2020; https://doi.org/10.1097/IAE.0000000000002760. [Epub ahead of print].
40. Huang CH, Yeh PT, Hsieh YT, Ho TC, Yang CM, Yang CH. Characterizing branching vascular network morphology in polypoidal choroidal vasculopathy by optical coherence tomography angiography. *Sci Rep* 2019;9(1):595.
41. Sadda SR, Guymer R, Holz FG, et al. Consensus definition for atrophy associated with age-related macular degeneration on OCT: classification of atrophy report 3. *Ophthalmology* 2018;125(4):537–548.
42. Yuzawa M, Mori R, Kawamura A. The origins of polypoidal choroidal vasculopathy. *Br J Ophthalmol* 2005;89(5):602–607.
43. Motulsky EH, Zheng F, Shi Y, Gregori G, Rosenfeld PJ. Anatomic localization of type 1 and type 2 macular neovascularization using swept-source OCT angiography. *Ophthalmic Surg Lasers Imaging Retina* 2018;49(11):878–886.
44. Zhang Q, Zheng F, Motulsky EH, et al. A novel strategy for quantifying choriocapillaris flow voids using swept-source OCT angiography. *Invest Ophthalmol Vis Sci* 2018;59(1):203–211.
45. Zhang M, Wang J, Pechauer AD, et al. Advanced image processing for optical coherence tomographic angiography of macular diseases. *Biomed Opt Express* 2015;6(12):4661–4675.